J. Fluid Mech. (1992), *vol.* 239, *pp.* 133–156
Printed in Great Britain

An experimental study of attenuation of short water waves by turbulence

By HASAN S. ÖLMEZ AND JEROME H. MILGRAM
Department of Ocean Engineering, Massachusetts Institute of Technology, Cambridge, MA 02139, USA

(Received 10 December 1990 and in revised form 14 November 1991)

Measurements of the dissipation of short water waves in a wave tank are analysed and described. Monochromatic waves with lengths between 6 and 10 cm generated by an axisymmetric wavemaker propagated through a turbulent flow field generated by a submerged vertically oscillating grid below the wavemaker. The horizontal turbulence velocity was measured with a hot-film anemometer with the grid oscillating, but the wavemaker off. With the wavemaker operating, wave amplitude *vs.* distance from the wavemaker was measured with and without operation of the turbulence generator. Wave dissipation due to turbulence was measured and quantified. Much of the wave energy transfer to turbulence may not occur in the normal energy-containing depth of the waves. Rather, most of it may first be convected downward and out of the wave zone by the vertical turbulent velocities. The experimental data are consistent with this possibility.

1. Introduction

Long-standing interest in the damping of short waves by turbulence has intensified in recent years because of the importance of short-wave dynamics for microwave remote sensing of the sea surface. Variable ocean currents, long gravity waves, internal waves, ship wakes and wind have little direct influence on microwave backscattering. They are all sensed indirectly by their influence on the short waves mainly responsible for the detectable backscattering. Turbulent wave dissipation plays only a minor role in measurements related to modulations of the short waves such as those of long waves and currents. On the other hand, turbulent wave dissipation can be particularly important for phenomena which change short-wave energy over substantial lengthscales such as remote measurement of ship wakes and estimation of wind speed by backscattered microwave intensity from the sea.

Turbulence influences water waves through both scattering and dissipation. Scattering can change the directions of waves and it is anticipated that interactions between waves and turbulent eddies of similar lengthscales can scatter wave energy into different wavelengths although we know of no detailed development of the theory for this phenomenon. As opposed to scattering, turbulent dissipation diminishes wave energy.

Phillips (1958) developed a theory for scattering of waves into different propagation directions by turbulence. In his Introduction, Phillips describes one dissipation mechanism whereby energy is transferred from the wave to the turbulence through a mean straining of the turbulence by the waves. He indicates that the mean strain in this process is proportional to the square of the wave steepness, leading to wave decay rates that increase with wave amplitude. (Whilst this is surely true for the low-frequency energy-containing turbulent eddies, the situation is less certain for the portion of the turbulence whose frequencies are much larger than the wave frequencies.) The scattering theory of Phillips conserves wave energy and transfers wave energy into altered wave directions at a rate proportional to the wave energy. This leads to decay rates of an incident wave that do not depend on wave amplitude, with the lost incident wave energy appearing in a wave with an altered direction.

Several investigations have focused on the decay of waves due to turbulence generated by the waves themselves. Skoda (1972) provides references to these investigations and describes them briefly in his Literature Survey. They base wave decay on an eddy viscosity which increases with increasing wave amplitude leading to a self-induced wave decay rate that depends on wave amplitude. This is somewhat different from the situation we shall consider where we want to learn the rate of wave decay due to prescribed turbulence.

Savitsky (1970) attempted to measure wave dissipation due to turbulence generated by a towed grid in a rectangular tank. However, as he explained, towing the grid, which did not span the width of the tank, set up shear layers which so strongly scattered the waves that the turbulence-induced wave dissipation could not be measured.

Boyev (1971) suggested that the turbulent motion could convect wave energy downward and out of the zone of wave motion with an associated wave decay rate that was independent of wave amplitude. The essence of this idea is that downward turbulent velocities at a prescribed depth could convect wave energy from above that depth to lower locations whereas upward turbulent velocities would convect less wave energy upward.

Green, Medwin & Paquin (1972) measured the dissipation of waves with frequencies of 2 to 10 Hz due to turbulence generated by a submerged horizontal grid that was oscillated vertically. The intensity of the turbulence shown in their figure 3 is unreasonably large in view of their grid oscillation parameters so we view it as unknown. However, they did measure and report wave damping rates due to the presence of the turbulence that were one to two orders of magnitude greater than the damping due to viscosity alone.

Green *et al.* calculated two mathematical forms of the wave amplitude damping rates due to turbulence. One was independent of wave amplitude and the other was proportional to wave amplitude. Although they concluded that the damping rate proportional to wave amplitude gave a better fit to the data, our study of the data does not indicate conclusively that one form is better than the other.

Skoda (1972) made laboratory measurements of the dissipation of mechanically generated monochromatic waves and of the effect of turbulence on the growth rate of wind-generated waves. It is difficult, if not impossible, to gain much understanding from Skoda's wind-wave experiments, but his data for the dissipation of monochromatic waves by turbulence conclusively demonstrate the effect. Skoda generated turbulence with submerged oscillating paddles and measured the horizontal turbulent velocities 4.5 cm beneath the surface with a hot-film anemometer. Experimental artifacts masked the turbulence spectrum for wavenumbers in excess of 1 cm^{-1}. However, an inertial subrange is seen to begin at a wavenumber of about 0.4 cm^{-1} with a relatively constant spectral level at lower wavenumbers.

Skoda's analysis and interpretation is confusing in that he relates measured dissipation to eddy viscosities formulated by others for wave-induced turbulence, whereas most of the turbulence was actually generated by the separate turbulence-generating paddles. Furthermore, he neglected the significant damping due to friction on the sidewalls of his wave channel. Nevertheless, the experiments do demonstrate wave dissipation in terms of reasonably defined turbulence conditions. We have carried out a reanalysis of Skoda's data which is explained in the Appendix. Although we included the effect of laminar wall friction in the reanalysis, the increase in wall damping due to the presence of the turbulence is completely unknown. To avoid this difficulty in our experiments, we used axisymmetric circular waves and completed each experimental run before waves reflected from any tank wall reached the wave sensor.

Kitaigorodskii & Lumley (1983) derived a theoretical treatment of the energy balance of wave–turbulence interactions in the upper ocean. Their equation (46) expresses the mean rate of change of turbulent energy per unit mass, e_t as

$$\frac{\partial e_\mathrm{t}}{\partial t} = -\frac{\partial}{\partial t}[\tfrac{1}{2}\langle|\boldsymbol{u}^\mathrm{w}|^2 w'] + \text{terms not involving the waves,} \tag{1}$$

where $\boldsymbol{u}^\mathrm{w}$ is the wave particle velocity vector, w' is the vertical component of the turbulence velocity, z is the vertical coordinate and $\langle\ \rangle$ represents the statistical average. The first term on the right-hand side is the divergence of the wave kinetic energy flux associated with convection of the wave energy by the turbulence velocity.

Kitaigorodskii & Lumley (1983) integrate (1) over z to obtain the mean rate of energy transfer, $\mathscr{R}$, per unit surface area from the waves to the turbulence, which must equal the wave energy loss rate:

$$\mathscr{R} = [\langle\tfrac{1}{2}\rho|\boldsymbol{u}^\mathrm{w}|^2 w'\rangle]_{z=0}, \tag{2}$$

where ρ is the water density and $z=0$ corresponds to the mean location of the surface. Kitaigorodskii & Lumley (1983) interpret (2) as the downward flux of wave kinetic energy of the wave motion associated with $|\boldsymbol{u}^\mathrm{w}|^2$ due to the turbulence velocity, w'.

Equation (2) is not meaningful with the right-hand side evaluated exactly at the free surface because w' is very nearly zero there (see below). However, if we integrate only up to a depth $z=\delta$, the result $\mathscr{R}(\delta)$ can be interpreted as the rate at which wave energy above $z=\delta$ is convected by w' to the region below $z=\delta$ where it is transferred to the turbulence. This is equivalent to the concept of Boyev explained above:

$$\mathscr{R}(\delta) = [\langle\tfrac{1}{2}\rho|\boldsymbol{u}^\mathrm{w}|^2 w'\rangle]_{z=\delta}. \tag{3}$$

We shall show how the concepts of Boyev and of Kitaigorodskii & Lumley (1983) can be applied to our wave decay measurements to relate wave decay to the structure of the turbulence. Although results of the reanalysis of Skoda's data show considerable scatter, they are, by and large, consistent with our formulation for the relation between wave decay and turbulence parameters.

1.1. *Structure of turbulence near a free surface*

Brumley & Jirka (1987) conducted measurements and analysis of turbulence in a laboratory 'mixing box' with a free surface, with the turbulence generated by a submerged oscillating grid. Both horizontal and vertical velocity components were measured over a range of depths up to within 0.4 mm of the surface.

The presence of the free surface altered the structure of turbulence, making it strongly anisotropic in a surface layer whose thickness was of the order of the integral lengthscale of the relatively isotropic turbulence beneath it. The turbulence structure

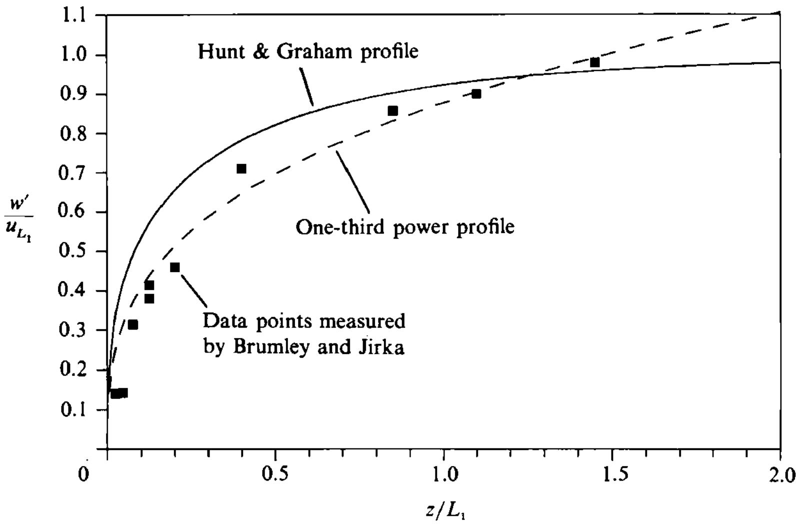

FIGURE 1. Profiles of vertical r.m.s. velocity. The one-third power-law profile is chosen to pass through w'/u_{L_1} at a depth of $1.5L_1$. u_{L_1} is the r.m.s. horizontal velocity at a depth of one longitudinal integral lengthscale.

was the same as found by others near the tops of closed mixing boxes, except for a surface boundary layer, much thinner than the aforementioned surface layer. In particular, the structure of the vertical velocity near the surface is in close agreement with

(*a*) the measurements in a closed mixing box made by McDougall (1979); and

(*b*) the theory of Hunt & Graham (1978) wherein the flow near the surface is the sum of the far-field turbulent velocity and an irrotational flow, generated by a 'surface source sheet', which cancels the vertical turbulent velocity at the surface.

We shall rely on knowledge of the structure of the near-surface turbulence found by Brumley & Jirka (1987) for analysing and interpreting our measurements. One reason for this is that we measured only the horizontal turbulence velocities and we need to relate these to the vertical velocities. Furthermore, we shall assume that the near-surface relationships between the horizontal and vertical turbulence velocities for grid-generated turbulence apply to the paddle-generated turbulence used by Skoda. This is reasonable since the depths of the turbulence-generating devices were much greater than the integral lengthscales. The turbulence characteristics for the fluid region from the surface down to 35% of the depth of the oscillating grid, important for our work here are:

(i) The measured r.m.s. horizontal velocity, u', is roughly constant in depth. Brumley & Jirka (1987) found increases of as much as 25% in parts of the region between 1 and 10% of the grid depth, but McDougall found increases of only 5% for the same region of his closed mixing box.

(ii) Calculations of the longitudinal integral lengthscale L_1 of the horizontal velocity show considerable scatter and their average is about 10% of the grid depth. There is a trend for slightly shorter values at depths less than 5% of the grid depth.

(iii) Measurements show the r.m.s. vertical turbulence velocity is nearly zero at the surface and increases with depth. At a depth of about 15 to 20% of the grid depth the vertical and horizontal r.m.s. velocities become roughly equal. Figure 1 shows the r.m.s. vertical velocity *vs.* depth measured by Brumley & Jirka (1987) (their figures 5 and 6), as well as the Hunt & Graham (1978) theoretical profile and a one-third power law which matches horizontal and vertical turbulence velocities at a depth of $1.5L_1$. The latter is a slightly better fit to the data and has a more convenient form for our subsequent analysis.

(iv) The vertical integral lengthscale, L_3, of the vertical velocity, is zero near the surface and increases with the cube root of depth till it becomes about 5% of the grid depth at a depth of 15% of the grid depth.

(v) All of the Brumley & Jirka measurements agree with the Hunt & Graham theory as well as can be expected in such a difficult and complicated experiment. An essential feature of the Hunt & Graham theory is that the vertical turbulent velocity is zero at the surface.

(vi) The overall picture of the turbulence is one which is isotropic at depths below 15 to 20% of the grid depth, which is 1.5 to 2 integral lengthscales of the horizontal velocity. Above this depth the horizontal turbulence velocity is altered only slightly by the presence of the surface. On the other hand, the surface has a strong influence on the vertical velocity and its lengthscale, diminishing both of them to essentially zero at the surface.

2. Apparatus

2.1. *Test tank and general experimental arrangement*

The experiments were conducted in the large tank in the Ship Hydrodynamics Laboratory at the University of Michigan. The tank is 110 m long, 6.7 m wide and has a depth that varies with transverse location, but which is everywhere in excess of 2 m. Figure 2 shows the general arrangements of the apparatus. A transverse steel bridge was installed over the tank. The mechanism for vertically oscillating the submerged grid and the axisymmetric wavemaker were attached to the bridge. The oscillation mechanism and the grid were connected by eight vertical rods with diameters of about 1 cm. The rods formed two longitudinal rows of four rods each.

The tank is equipped with a powered carriage and an unpowered subcarriage, both supported by wheels riding on common tracks running the length of the tank. The two carriages were connected together with a 9 m steel beam which passed beneath the bridge and between the two rows of vertical connecting rods. Since neither carriage could pass the bridge, this arrangement allowed about 7 m of carriage run length.

To measure turbulence, a hot-film anemometer sensor was attached to the steel beam and the carriage was run at a speed of 50 cm/s while the sensor passed over the grid. To measure waves, the carriage was kept stationary and a wave gauge was attached to the steel beam at a prescribed location. For each wave and turbulence condition, several locations spaced 30.5 cm (1 ft) apart, starting 30.5 cm from the wavemaker axis were used. All the measured wave and turbulence signals were digitized and recorded on computer diskettes in real time.

2.2. *Surface cleaning*

If any surface films were present, they could strongly damp the short waves we were measuring so a surface film removal system was installed. It consisted of a perforated pipe spanning the width of the tank on the bottom under the location where we made wave and turbulence measurements. When an air supply was attached to the pipe, air coming out of the perforations generated a 'two-dimensional' bubble plume which rose and spread longitudinally in both directions at the surface. The entrained water became diverging longitudinal currents which swept surface material away

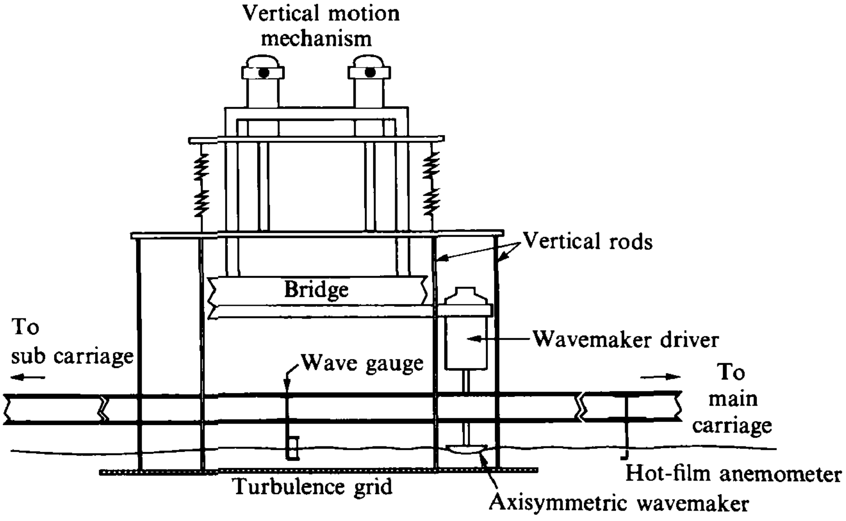

FIGURE 2. Experimental apparatus arrangement.

from the measurement region. Skimmers located along the tank sides about 20 m away from the measurement region removed the surface material. This system was operated for lengthy periods of time when experimental measurements were not being made and turned off 15 min prior to any measurements. By that time the currents had diminished to the extent that they could not be detected by eye.

Surface contamination was monitored by measurements of the surface tension. After installation and use of the surface film removal system, the measured surface tension was never less than 0.5 dynes/cm less than that of pure water at the same temperature. Prior to installation of the surface cleaning system and initiation of surface film monitoring, uncertain and unpredictable wave damping results were obtained.

2.3. *Turbulence generator*

A rectangular grid with dimensions of 2.44 × 3.05 m (8 × 10 ft) at a mean depth of 20 cm was oscillated vertically to generate the turbulence. The grid was made of expanded metal having openings of about 3 × 6 cm which was covered with a wooden lattice having slat widths of 3.8 cm on 10.2 cm centres. The resulting grid had a solidity of 56%. For each experimental run, the grid was driven in sinusoidal motion with a frequency of either 0.62 or 0.90 Hz and with an amplitude between 1.25 and 5.0 cm.

2.4. *Axisymmetric wavemaker*

Axisymmetric waves were generated by vertically oscillating one of two surface-piercing bowl-shaped forms. Most of the experiments were done with a bowl whose waterplane radius was about 9 cm. To determine the effect of larger wave amplitudes a few experiments were done with a bowl whose waterplane radius was about 14 cm. The bowls were driven in sinusoidal motion with amplitudes of a few mm and at frequencies between 4.0 and 5.3 Hz.

2.5. *Turbulence measurements*

Horizontal turbulent velocity fluctuations were measured by a constant-temperature hot-film anemometer with a quartz-coated conical type hot-film sensor. Calibration data were obtained by operating the carriage over a range of speeds with calm water.

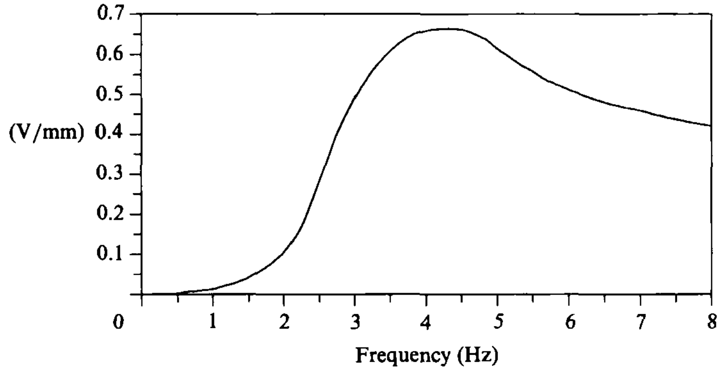

FIGURE 3. Frequency response of the wave measurement system.

Although the anemometer had a built-in linearizer, the output was not exactly linear with velocity. Actual velocities were obtained by using the measured calibration data in the computer program which analysed the data.

2.6. *Wave measurements*

Wave elevations were measured at 6 or 8 locations with a resistance-type wave gauge made of two parallel 30-gauge nichrome wires spaced 3 mm apart. The gauge was sequentially moved to each measurement location. Output signals went directly to a 12-bit A-to-D converter. In addition to the high-frequency waves being measured, whose amplitudes varied from a fraction of a mm to a few mm, the grid motion generated lower frequency waves with an amplitude of about 1 cm. In order to use most of the dynamic range of the A-to-D converter for the high-frequency waves, the wave-gauge electronics contained filters that suppressed low frequencies, amplified the frequencies of interest and suppressed still higher frequencies so the data sampled at 200 Hz would not be aliased. The wave gauge was calibrated by oscillating it sinusoidally in calm water over a range of frequencies. Figure 3 shows the calibration in the frequency range of interest.

3. Experimental procedures

The experimental procedure was as follows:

(i) If the bubble-plume surface cleaning system was operating prior to any measurements, it was shut down and the currents were allowed to decay to less than 0.3 cm/s as judged by watching small plastic floating chips placed on the surface which were then removed.

(ii) The grid oscillation was started with a prescribed oscillation frequency and amplitude.

(iii) After the grid had run for two or more minutes the hot-film anemometer was towed at a speed of 50 cm/s through the turbulent zone above the grid. Turbulence statistics were found to be stationary after the grid had run for more than one minute. Data were acquired for 4 s and digitized at a rate of 300 Hz. Three of these turbulence data-acquisition runs were made for each grid oscillation condition. This step was done with anemometer probe depths of 1.9, 2.5, 3.8 and 7.6 cm beneath the free surface.

(iv) The grid was stopped, the water was allowed to become calm and then steps (ii) and (iii) were repeated for a different combination of grid frequency and amplitude. This was continued until measurements were obtained for grid amplitudes of 1.3, 1.9, 2.5, 3.8 and 5.1 cm at a grid frequency of 0.62 Hz, and amplitudes of 1.3, 1.9, 2.5 and 3.8 cm at a frequency of 0.90 Hz.

(v) The grid oscillation was stopped and the wavemaker was lowered into the water. The wave measurement sensor was located 30.5 cm (1 ft) from the wavemaker axis.

(vi) Next wave elevations were determined in the absence of turbulence. When the water became calm, the wavemaker was started. When the waves reached the wave sensor, surface elevation was measured for 10.24 s and digitized at a rate of 200 Hz. The 10.24 s interval was completed before waves reflected off the nearest tank wall reached the wave sensor. The wavemaker was stopped and when the water became calm this step was repeated two more times so three data records were made for each condition. The wavemaker stroke of roughly 3 mm varied slightly with frequency, but was held constant for all tests at each frequency (4.03, 4.17, 4.50, 4.95 or 5.27 Hz).

(vii) The wave sensor was moved 30.5 cm further from the wavemaker axis and the above step was repeated. This process continued until three data records were acquired at each of six or more locations.

(viii) The turbulence generator was started at one of the prescribed combinations of grid frequency and amplitude and the above process of acquiring surface elevation data was repeated with the wavemaker at rest. The reason for this is that the grid motion led to very small turbulence-related surface motions and a larger wave-like motion at the grid frequency and its first few harmonics. The resulting surface motions formed a background against which the waves measured in the next step were evaluated.

(ix) With the turbulence generator running, the wavemaker was turned on and the measurements of steps (vi) and (vii) were repeated to determine the wave motion *vs.* radius in the presence of turbulence.

(x) Steps (vi)–(ix) were carried out for wave frequencies of 4.03, 4.17, 4.50, 4.95 and 5.27 Hz for a range of turbulence conditions using the small bowl wavemaker. They were also carried out with the large bowl wavemaker for two sets of conditions in order to assess the effect of wave amplitude.

4. Data analysis

4.1. *Analysis of horizontal turbulence velocities*

The horizontal velocity measurements were processed into wavenumber spectra where the 'frozen turbulence' approximation was used to transform the frequency spectra into wavenumber spectra. This relates wavenumbers to frequencies by

$$k = \frac{2\pi}{U_p} f, \tag{4}$$

where U_p is the towing speed.

During measurements of the turbulence with the hot-film anemometer, the fluid motion was the sum of the turbulence and a wave-like motion centred mainly at the grid oscillation frequency. This latter motion resulted from a spatially averaged motion of some of the water above the grid moving vertically in phase with the grid. (This motion does not occur in a mixing box with the grid spanning the planform of the box for which the spatially averaged vertical velocity must be zero.) Outside the longitudinal extent of the grid, the motion mainly took the form of longitudinal waves. At one end of the tank these waves were absorbed by a beach, but at the other end the waves were reflected by a wall so that small-amplitude long waves as well as the general up-and-down motion existed over the grid. The amplitude of the surface motion was typically 1 cm or less.

Separation of the turbulence spectrum from the total spectrum was based on the fact that the turbulence spectrum should be nearly constant at wavenumbers significantly below the cutoff wavenumber, k_c,

$$k_c = 1/L_1. \tag{5}$$

Our grid depth was 20 cm and since the horizontal integral lengthscale is about 10% of this depth, $L_1 \approx 2$ cm. This leads to

$$k_c \approx 0.5 \text{ cm}^{-1} \quad \text{or} \quad f_c \approx 4 \text{ Hz}, \tag{6}$$

where f_c is the cutoff frequency.

We replaced spectral values for frequencies less than 2.1 Hz by the first calculated value above 2.1 Hz. This removed the grid motion fundamental and its first harmonic for a grid frequency of 0.9 Hz and the fundamental and its first two harmonics for a grid frequency of 0.62 Hz.

The steps taken to generate the spectra were as follows. First the three measurement records obtained for a prescribed turbulence condition were labelled $u_j(t), j = 1, 2, 3$. The Fourier transform, $U_j(f)$ was obtained for each record from 1024 data points corresponding to a record length of $T = 3.413$ s. Secondly, raw one-sided frequency power spectra, $S_r(f)$ were taken as

$$S_r(f) = \begin{cases} \dfrac{1}{3}\displaystyle\sum_{j=1}^{3} 2\dfrac{|U_j(f)|^2}{T} & \text{if} \quad f > 2.1 \text{ Hz} \\ S_c & \text{if} \quad f \leqslant 2.1 \text{ Hz}, \end{cases} \tag{7}$$

where S_c if the value of S_r at 2.34 Hz, which is the first value above the cutoff frequency provided by the FFT algorithm. The factor of 2 makes the spectrum one-sided.

Thirdly, smoothed frequency spectra, $S_s(f)$, were generated by convolving the raw spectra with a Parzen spectral window (cf. Jenkins & Watts 1968, Ch. 6) whose corresponding autocorrelation window length is $\frac{1}{4}T$:

$$S_s(f) = S_r(f) \otimes \tfrac{3}{16}T\left[\frac{\sin(\frac{1}{8}\pi fT)}{\frac{1}{8}\pi fT}\right]^4. \tag{8}$$

Confidence limits for the spectral estimates correspond to about 45 degrees of freedom since the Parzan window used provides 15 degrees of freedom and three spectra have been averaged together. The spectra were truncated at $f_{\max} = 50$ Hz, which corresponds to $k_{\max} = 6.28$ cm^{-1} at which spectral levels were roughly 2% of their low-frequency values.

Finally, wavenumber spectra, $S(k)$, were made from the frequency spectra using

$$S(k) = \frac{U_p}{2\pi}[S_s(f)]_{f=(U_p/2\pi)k}. \tag{9}$$

As an example, figure 4 shows turbulence spectra for one turbulence condition at depths of 1.9, 2.5 and 3.8 cm. The latter depth range exceeds one-quarter of a wavelength of waves used in the experiment. 95.7% of the wave kinetic energy is

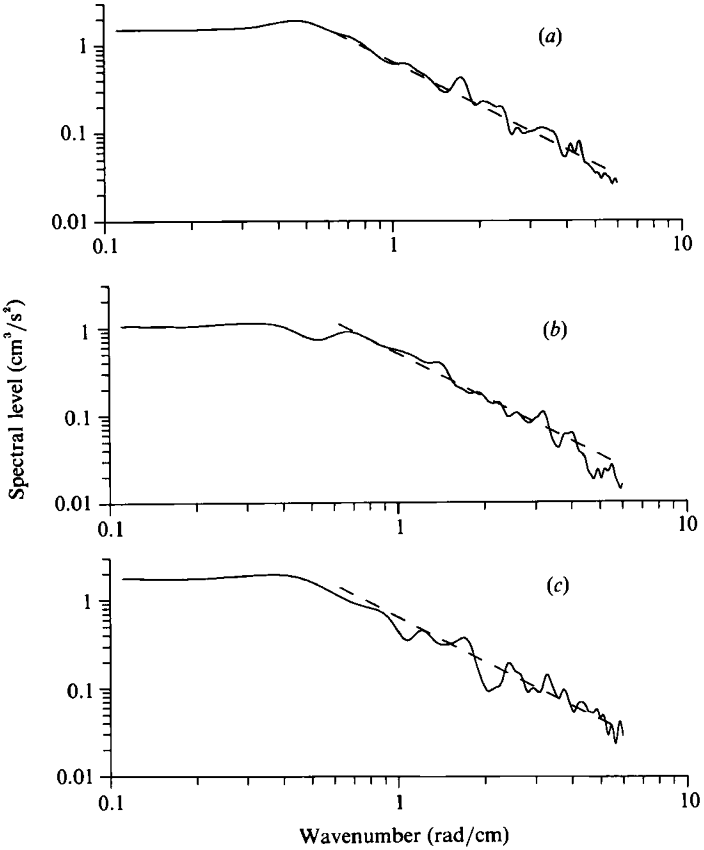

FIGURE 4. Turbulence spectra for grid oscillation at 0.90 Hz with an amplitude of 1.9 cm: solid line is from experimental data; dashed line is a $k^{-\frac{5}{3}}$ fit to the inertial subrange. (*a*) Probe depth = 19 mm, (*b*) 25 mm, (*c*) 38 mm.

contained in the layer one-quarter of a wavelength deep. Notable observations from the figure are that in the inertial subrange the spectra behave nearly as $k^{-\frac{5}{3}}$ and there is small variation in energy level in the three measurements. These features appeared in all the measurements. For the example shown in figure 4 the spectral level at a depth of 2.5 cm is less than at either more or less depths. This is due to spectral variability and not a common trend since the lowest measured energy appears at all three measurement heights throughout the data set for the various conditions. Therefore, we shall consider the horizontal turbulence spectrum in the upper 3.8 cm of the water to be the average of the spectra at the three heights. Since the spectra at each height are based on three experimental runs, a total of nine individual spectra are averaged together for each turbulence condition.

The r.m.s. horizontal turbulence level, u', and the horizontal integral lengthscale, L_1, associated with each spectrum were determined by

$$u' = \left[\int_0^{k_{\max}} S(k)\,\mathrm{d}k\right]^{\frac{1}{2}}, \tag{10}$$

$$L_1 = \frac{\pi S(0)}{2(u')^2}. \tag{11}$$

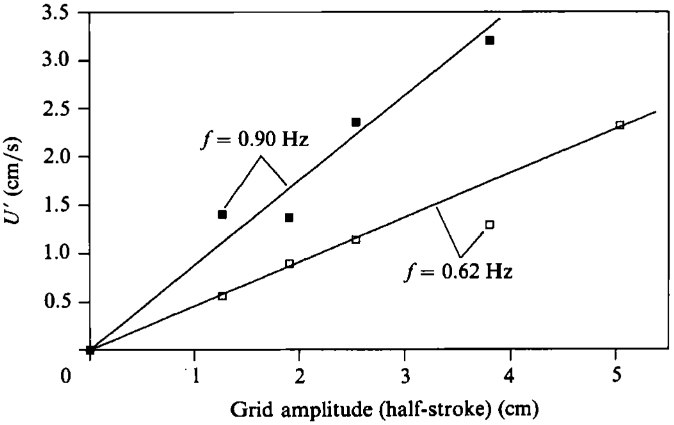

FIGURE 5. Calculated values of r.m.s. turbulence velocity and approximations that depend linearly on grid amplitude.

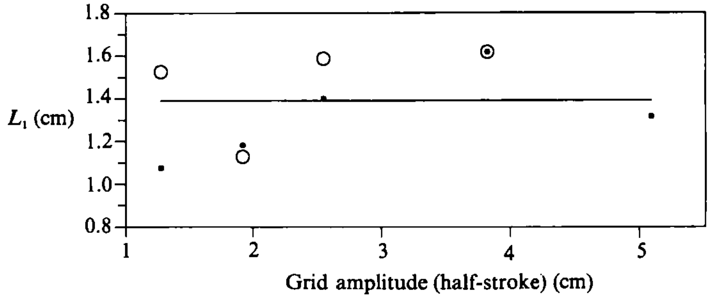

FIGURE 6. Calculated values of integral lengthscale, L_1, and its approximation by a constant (solid line). •, Grid frequency 0.62 Hz; ○, 0.90 Hz.

The calculated values of u' and L_1 are influenced by spectral variability and experimental error. Variability in our final results is diminished by using approximations to u' and L_1 which are smooth functions of grid amplitude.

Figure 5 shows the values determined for u' for various values of grid amplitude, A_g, and grid frequency f_g, as well as the approximations:

$$u' = \begin{cases} 0.46(\mathrm{s}^{-1})A_g & \text{if } f_g = 0.62\ \mathrm{Hg} \\ 0.88(\mathrm{s}^{-1})A_g & \text{if } f_g = 0.90\ \mathrm{Hz}. \end{cases} \tag{12}$$

In forming the approximations in (12), the point for 3.8 cm grid amplitude at a grid frequency of 0.62 Hz was ignored since it seems to be out of line with the others. Values for u' in our subsequent analysis are taken from (12), which provides a form of data smoothing.

Figure 6 shows calculated values of the integral lengthscale, L_1. Although there is a slight trend towards values that increase with grid amplitude, the effect is not significant over the range of conditions in our experiments. As a result, we shall use the average of the calculated values, 1.39 cm, in our subsequent analysis.

4.2. *Analysis of surface elevation measurements*

4.2.1. *Wave energy densities*

This analysis provided wave energy (mean-square surface elevation) *vs.* radius from the wavemaker for each wave condition both with and without the presence of turbulence. Doing this required accounting for both the very small vertical surface

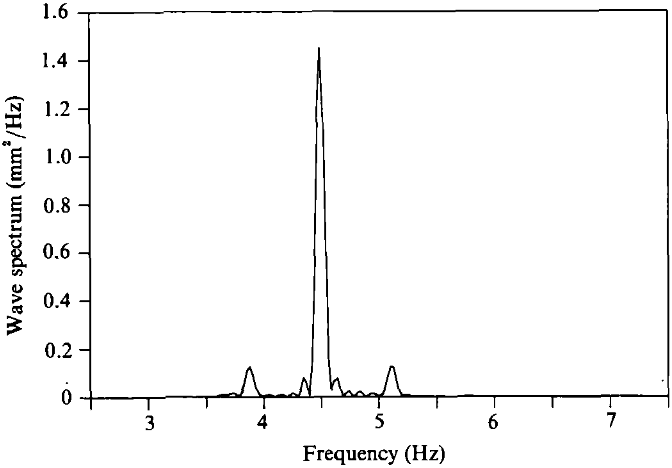

FIGURE 7. Wave spectrum 30.5 cm from the wavemaker axis with the wavemaker operating at 4.5 Hz and the grid moving with an amplitude of 1.9 cm at 0.62 Hz.

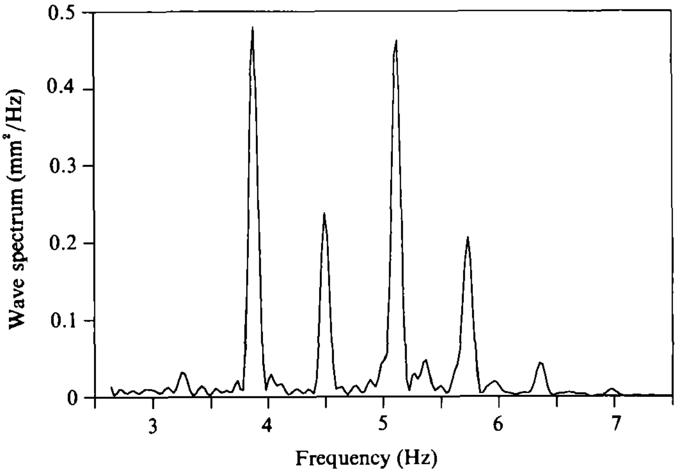

FIGURE 8. As figure 7 but with the grid moving with an amplitude of 3.8 cm at 0.62 Hz.

motions due to the turbulence and its generator in the wave frequency band and the occasionally larger modulations of the waves. These effects are best exemplified in the power spectra with both waves and turbulence present, $S_{\mathrm{wt}}(f)$, defined as

$$S_{\mathrm{wt}}(f) = \frac{1}{3}\frac{1}{T_{\mathrm{r}}}\sum_{n=1}^{3} 2\left|\int_{0}^{T_{\mathrm{r}}} z_n(t)\,\mathrm{e}^{\mathrm{i}2\pi ft}\,\mathrm{d}t\right|^2, \tag{13}$$

where the record length $T_{\mathrm{r}} = 10.24$ s, the initial factor of 2 makes the spectrum one-sided, and z_1, z_2, and z_3 are the data records from the three sets of measurements made for each wave turbulence condition. Corresponding surface elevation spectra, S_{wo} for only the wavemaker operating and S_{g} for only the turbulence grid operating are defined similarly.

Figure 7 shows a wave spectrum 30.5 cm from the wavemaker axis. It has the expected large peak at the wave frequency of 4.5 Hz and small side lobes 0.146 Hz on each side of the spectral peak due to the 10.24 s record length. In addition, the

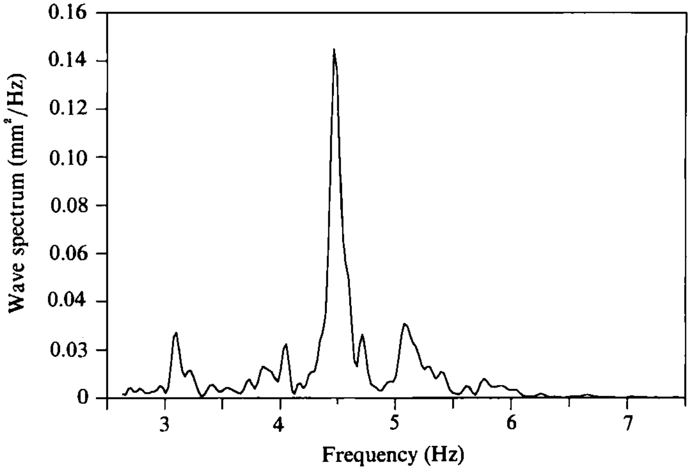

FIGURE 9. Wave spectrum 61 cm from the wavemaker axis with the wavemaker operating at 4.5 Hz and the grid moving with an amplitude of 3.8 cm at 0.62 Hz.

figure shows spectral peaks located at 4.5 ± 0.62 Hz. These occur because when the bulk up-and-down fluid motion caused by the grid oscillation at 0.62 Hz interacts with the bowl-shaped wavemaker, a local oscillating radially directed current occurs. The current causes amplitude and frequency modulations of the waves. Although the amplitude modulations are modest and relatively balanced between components that are shifted up and down in frequency, restricting the measurement frequency band to a narrow one at the wavemaker frequency could omit a substantial part of the wave energy. The frequency-modulated sidebands are larger when the grid amplitude is larger as shown in figure 8, for which the grid amplitude was increased from 1.9 to 3.8 cm. In this case the nearest sidebands are even more energetic than the 4.5 Hz peak and several additional sidebands with a spacing of 0.62 Hz are evident. The radial current modulating effect diminishes with distance from the wavemaker as shown in figure 9. This has the same conditions as figure 8 except that the wave measurements were made 61 cm from the wavemaker axis.

In figure 9 spectral peaks have broadened, probably due to wave modulation by the turbulence, while the waves propagate over the larger distance. Also, the spectral energy has diminished because of the $1/r$ attenuation of the cylindrical wave energy density and the dissipation. This leads to the background level due to the small turbulence-induced surface motions becoming a larger fraction of the total measured energy.

To take into account the influences on the wave spectra described above, the following steps were taken. First each combination of turbulence condition, wave condition and measurement location involved three spectra, one with both the wavemaker and the turbulence generator in operation, one with only the wavemaker running and one with only the turbulence generator operating. Each of these spectra was taken as the average of three sets of measurements as indicated in (13).

Then the surface elevation energy, E_{wt}, for each wave–turbulence condition was approximated by the integral of the corresponding spectrum between 3 and 7 Hz.

$$E_{\mathrm{wt}} = \int_{3\,\mathrm{Hz}}^{7\,\mathrm{Hz}} S_{\mathrm{wt}}(f)\,\mathrm{d}f. \qquad (14)$$

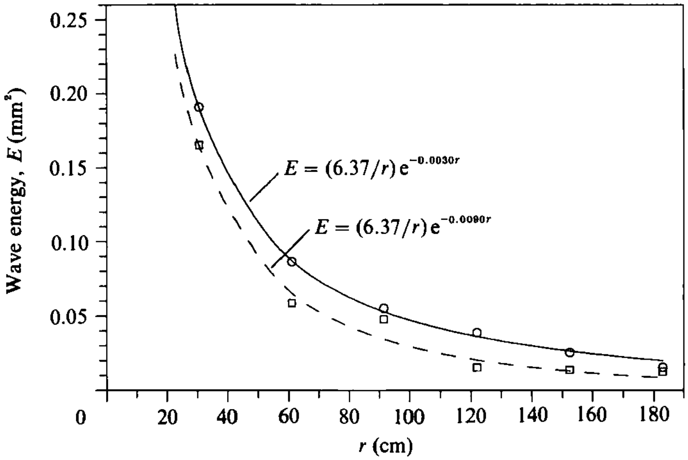

FIGURE 10. Data points and approximating functions for wave energy *vs.* distance from wavemaker axis at a grid frequency of 0.90 Hz, grid amplitude of 1.9 cm, and wave frequency 4.50 Hz. ○, Data with no turbulence; □, data with turbulence. The results for this case are $\beta_0 = 0.0015\ \text{cm}^{-1}$, $\beta_m = 0.0045\ \text{cm}^{-1}$, $\beta = 0.0030\ \text{cm}^{-1}$ and $\sigma = 0.059\ \text{s}^{-1}$.

ID 6					ID 12				
Waves and turbulence			Waves only		Waves and turbulence			Waves only	
E_w (mm^2)	$\tilde{E}_w$ (mm^2)	r (cm)	E_{wo} (mm^2)	$\tilde{E}_{wo}$ (mm^2)	E_w (mm^2)	$\tilde{E}_w$ (mm^2)	r (cm)	E_{wo} (mm^2)	$\tilde{E}_{wo}$ (mm^2)
0.1288	0.1427	30.5	0.1567	0.1572	0.1653	0.1651	30.5	0.1910	0.1907
0.0763	0.0622	61.0	0.0758	0.0755	0.0585	0.0652	61.0	0.0863	0.0869
0.0410	0.0361	91.4	0.0498	0.0483	0.0477	0.0343	91.4	0.0552	0.0529
0.0324	0.0236	121.9	0.0328	0.0348	0.0151	0.0203	121.9	0.0387	0.0361
0.0400	0.0165	152.4	0.0250	0.0267	0.0136	0.0128	152.4	0.0254	0.0264
0.0515	0.0120	182.9	0.0190	0.0214	0.0125	0.0084	182.9	0.0154	0.0200
0.0443	0.0089	213.4	0.0184	0.0176	Fit error			Fit error	
0.0157	0.0068	243.8	0.0187	0.0148	= 0.0079 (4)			= 0.0024	
Fit error			Fit error		Mean E_g = 0.0043			SD E_g = 0.0002	
= 0.0111 (4)			= 0.0020						
Mean E_g = 0.0177			SD E_g = 0.0037						

TABLE 1. Measured energy levels, E_w and E_{wo} and their approximations $\tilde{E}_w$ and $\tilde{E}_{wo}$. Following the energy *vs.* distance data, for each run the r.m.s. of the differences between the experimental data and their approximations are given and labelled 'Fit error'. For the data in the presence of turbulence, the number of data points used in generating the approximation and calculating the fit error is given in parenthesis. The following line shows the mean and standard deviation of the turbulence energy levels, E_g. The total data set contains 15 sets of test conditions. Only two sets are provided here because of the amount of detail involved with all 15 sets. The entire table of these data is available from the authors or the editor. Test conditions for each ID number are shown in table 2.

Surface elevation energies, E_{wo} and E_g for waves only or grid motion only were calculated in similar fashion.

Finally, the wave energy in the absence of turbulence was taken as E_{wo}. The wave energy in the presence of turbulence, E_w, was based on the increase in surface

ID	Grid freq. (Hz)	Grid amp. (cm)	f_w (Hz)	λ (cm)	c_g (cm^{-1} s)	P (cm^3)	β_m (cm^{-1})	β_0 (cm^{-1})	β (cm^{-1})	σ (s^{-1})	$\frac{u'}{L_1^{\frac{1}{3}}\lambda^{\frac{2}{3}}}$ (s^{-1})	$\frac{\sigma L_1^{\frac{1}{3}}\lambda^{\frac{2}{3}}}{u'}$	$\frac{\lambda}{L_1}$	$k_w A_w$	$\frac{f_w L_1}{u'}$
1	0.62	1.27	4.50	8.08	19.69	0.064	0.00164	0.00152	0.00013	0.003	0.128	0.020	5.81	0.039	10.87
2	0.62	1.90	4.50	8.08	19.69	0.064	0.00293	0.00152	0.00141	0.028	0.195	0.143	5.81	0.039	7.14
3	0.62	3.81	4.50	8.08	19.69	0.050	0.00244	0.00157	0.00087	0.017	0.389	0.044	5.81	0.035	3.58
4	0.62	3.81	5.27	6.06	18.35	0.039	0.00434	0.00137	0.00297	0.054	0.471	0.115	4.36	0.041	4.19
5	0.62	3.81	4.03	9.88	21.06	0.051	0.00155	−0.00010	0.00164	0.035	0.340	0.102	7.10	0.029	3.20
6	0.62	3.81	4.50	8.08	19.69	0.271	0.00214	0.00023	0.00190	0.037	0.389	0.096	5.81	0.081	3.58
7	0.62	3.81	4.50	8.08	19.69	0.064	0.00354	0.00152	0.00202	0.040	0.389	0.102	5.81	0.039	3.58
8	0.62	3.81	4.17	9.29	20.57	0.050	0.00225	0.00067	0.00158	0.033	0.355	0.092	6.68	0.030	3.32
9	0.62	5.08	4.50	8.08	19.69	0.064	0.00428	0.00152	0.00276	0.054	0.512	0.106	5.81	0.039	2.72
10	0.90	1.27	4.95	6.77	18.78	0.028	0.00180	0.00090	0.00090	0.017	0.281	0.060	4.87	0.031	6.14
11	0.90	1.27	4.50	8.08	16.69	0.064	0.00362	0.00152	0.00210	0.041	0.249	0.166	5.81	0.039	5.59
12	0.90	1.90	4.50	8.08	19.69	0.064	0.00453	0.00152	0.00302	0.059	0.374	0.159	5.81	0.039	3.72
13	0.90	2.54	4.50	8.08	19.69	0.064	0.00388	0.00152	0.00237	0.047	0.491	0.095	5.81	0.039	2.84
14	0.90	3.81	4.95	6.77	18.78	0.200	0.00479	0.00053	0.00426	0.080	0.840	0.095	4.87	0.083	2.05
15	0.90	3.81	4.95	6.77	18.78	0.028	0.00638	0.00090	0.00548	0.103	0.840	0.123	4.87	0.031	2.05

TABLE 2. Quantities calculated from the experimental measurements. In forming the ratios on the right-hand side of the table, L_1 was taken as the average value of 1.39 cm (figure 6) and u' was obtained from equation (12) (shown in figure 5). For evaluating $k_w A_w$, A_w was taken as $[2P/(50\text{ cm})]^{\frac{1}{2}}$. This is the wave amplitude at a radius of 50 cm in the absence of any dissipation.

elevation energy when the wavemaker was operated in the presence of the background turbulence, so

$$E_{\mathrm{w}} = E_{\mathrm{wt}} - E_{\mathrm{g}}. \tag{15}$$

Values for E_{wo} and E_{w} *vs.* distance from the wavemaker axis are given in table 1 for two sets of experimental conditions.

4.2.2. *Estimation of decay rates*

For each turbulence and wave condition, the foregoing procedure provided values of wave energy at 6 or 8 radii, both with and without the presence of turbulence, $E_{\mathrm{w}}(r_n)$ and $E_{\mathrm{wo}}(r_n)$ respectively. In each case, we first fit the values of E_{wo} with a function $\tilde{E}_{\mathrm{wo}}(r)$,

$$\tilde{E}_{\mathrm{wo}}(r) = \frac{P}{r}\mathrm{e}^{-2\beta_0 r} \tag{16}$$

where P and β_0 were chosen to minimize the mean-square error between the function $\tilde{E}_{\mathrm{wo}}(r_n)$ and the data points, $E_{\mathrm{wo}}(r_n)$.

Then, for the same wavemaker motion, but with turbulence present, two alternative estimation procedures are to fit values of E_{w} with the function $\tilde{E}_{\mathrm{w}}(r)$ or with the function $\hat{E}_{\mathrm{w}}(r)$,

$$\tilde{E}_{\mathrm{w}}(r) = \frac{P}{r}\mathrm{e}^{-2\beta_{\mathrm{m}} r}, \tag{17}$$

$$\hat{E}_{\mathrm{w}}(r) = \frac{P_{\mathrm{m}}}{r}\mathrm{e}^{-2\beta_{\mathrm{m}} r}. \tag{18}$$

For the first alternative, identical wavemaker motions are assumed to generate initially identical waves with and without the presence of turbulence and β_{m} is chosen to minimize the mean-square error between $\tilde{E}_{\mathrm{w}}(r_n)$ and the data points $E_{\mathrm{w}}(r_n)$. For the second alternative both P_{m} and β_{m} are chosen such that the error is minimized. We have tested both alternatives with the finding that the second leads to much more scatter in the results than the first. One contributor to this is the variability in the mean-square surface motion associated with the turbulence. As shown in table 1, the mean of the measured values of E_{g} is comparable with, and sometimes larger than, E_{w} at the larger measurement radii. The data scatter is reduced by using results at only the three smallest radii for the analysis, but the scatter is still larger than for the first alternative. Values for P_{m} for minimum error are smaller than P in some cases and larger in others. Because of these findings, we have chosen the first alternative, (17), for the remainder of the data analysis.

When the dissipation was especially rapid, only the first 4 or 5 data points were used in minimizing the error. The spatial decay rate of wave amplitude due to the turbulence, β was taken as

$$\beta = \beta_{\mathrm{m}} - \beta_0. \tag{19}$$

Finally, the temporal decay rate of wave amplitude due to the turbulence σ was taken as:

$$\sigma = \beta c_{\mathrm{g}} \tag{20}$$

where c_{g} is the group velocity of the waves.

Figure 10 shows an example of the data and the approximating functions for one set of wave and turbulence conditions. Calculated values of P, β_{m}, β_0, β and σ are shown in table 2.

5. Relationship between turbulence and wave decay rates

5.1. *Parameterization of experimental results*

We presume that the decay rate of waves in turbulence is mainly dependent, at most, on the wave parameters of amplitude A_w, wavelength λ, and wave frequency f_w; and the turbulence parameters. We consider wavelength and frequency as independent variables rather than just one of them plus gravity and surface tension together setting the other. Statistics of the horizontal turbulent velocities are expected to be relatively constant and parameterized by u' and L_1 throughout the depth of short-wave energy. Statistics of the vertical velocity, however, vary with depth, z, in the short-wave energy zone. On the basis of the studies cited in §1, we approximate the r.m.s. vertical turbulence velocity, w', at depth z by

$$w'(z) = u'\left[\frac{z}{1.5L_1}\right]^{\frac{1}{3}}. \tag{21}$$

The relationship between the turbulence-induced wave decay rate, σ, and the wave and turbulence parameters can be described by

$$\sigma = F[u', L_1, f_w, \lambda, A_w], \tag{22}$$

which has the equivalent non-dimensional form

$$\frac{\sigma\lambda^{\frac{2}{3}}L_1^{\frac{1}{3}}}{u'} = \mathscr{F}\left[\frac{\lambda}{L_1}, k_w A_w, \frac{f_w L_1}{u'}\right], \tag{23}$$

where $k_w \equiv 2\pi/\lambda$. The fractional exponents on the left-hand side of (23) are not unique. Any two that add up to 1 will do. However, the choice shown makes the left-hand side proportional to the ratio of the wave decay rate to the turbulence mixing rate, $\mathscr{M}$. $\mathscr{M}$ is proportional to the inverse of the time required for the vertical turbulent velocity at a depth that is a fixed fraction, μ, of a wavelength to move fluid vertically by the same distance, $\mu\lambda$:

$$\frac{w'(\mu\lambda)}{\mu\lambda} \sim \frac{u'}{L_1^{\frac{1}{3}}\lambda^{\frac{2}{3}}} \equiv \mathscr{M}. \tag{24}$$

Figure 11 shows our turbulent decay rates σ *vs.* the mixing rate, $\mathscr{M}$, and its best 'straight-line fit',

$$\sigma = 0.103\frac{u'}{L_1^{\frac{1}{3}}\lambda^{\frac{2}{3}}}. \tag{25}$$

If (25) were strictly true, the independent non-dimensional parameters on the right-hand side of (23) would not be influential. Table 2 shows values of the four non-dimensional parameters in (23) for the various wave and turbulence conditions in our experiment. (Procedural difficulties led to unreliable wave data for the turbulence condition generated by a grid amplitude of 2.5 cm at a frequency of 0.62 Hz. The wave data for this condition are not included in the analysis.) No clear trend can be detected in the data for influences in the right-hand side parameters.

Our data include only fractional variations in λ/L_1 so we cannot assess the influence of this parameter from the data alone. The parameter $f_w L_1/u'$ is the ratio of the wave frequency to the characteristic turbulence frequency. In assessing the influence of this parameter, we discount the first point in table 2 because it is

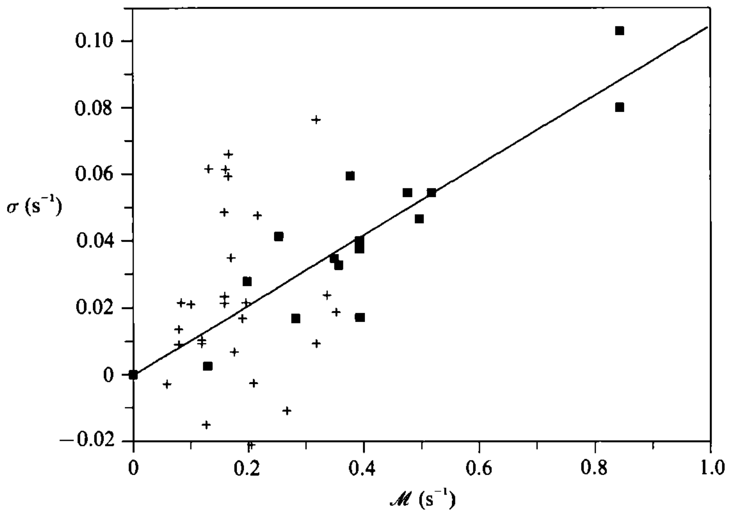

FIGURE 11. Turbulence-induced wave decay rates *vs*. turbulent mixing rate: ■, our data; +, reanalysis of Skoda data; ——, best straight line fit to our data; r.m.s. decay rate error in fit = 0.0109 s^{-1}. Two of Skoda's data points lie above the figure and are not shown.

associated with such a small decay rate that its determination is subject to substantial percentage error. For all the other points, $f_w L_1/u'$ varies between 2.0 and 7.2. This covers variations by more than factor of three without a discernible trend for its influence on $\sigma\lambda^{\frac{2}{3}}L_1^{\frac{1}{3}}/u'$. Likewise, values of $k_w A_w$, which are small and vary by a factor of nearly three, exert no observable trend on $\sigma\lambda^{\frac{2}{3}}L_1^{\frac{1}{3}}/u'$. Thus, (25) is the best estimate we can make for the relation between turbulence and wave decay rates from our data.

Figure 11 also shows decay rates obtained by our reanalysis of Skoda's data. These points have considerable scatter and include damping from the unquantified influence of turbulence on dissipation in the channel sidewall boundary layers. Nevertheless, they do agree in order of magnitude with (25).

6. Discussion of the decay rate relation

Equation (25) is the best approximation we can make for the functional form for the decay rate expressed by (23). A potentially significant weakness in the approximation occurs because our data do not cover a wide enough range in λ/L_1 to assess the influence of this factor alone. If such an influence were to exist, the wave damping might not be proportional to $u'/(L_1^{\frac{1}{3}}\lambda^{\frac{2}{3}})$ which could affect conclusions about the dominant physical mechanisms causing wave decay. However, by means of an order-of-magnitude calculation, we can show that the decay rate which would be caused by the downward convection of wave energy by turbulence has reasonable numerical consistency with (25).

Suppose we approximate the probability distribution function for the vertical turbulence velocity, $p(w)$, as Gaussian and define the mean downward turbulence velocity, w_d as

$$w_d \equiv \int_0^\infty w p(w)\,dw = \frac{w'}{(2\pi)^{\frac{1}{2}}}. \tag{26}$$

At a depth which is a fraction, μ, of the wavelength, the rate of downward convection of kinetic energy per unit area, $\mathscr{Q}$, is expected to be proportional to w_d and the mean kinetic energy density above the depth $\mu\lambda$:

$$\mathscr{Q} = \gamma(\mu)\, w_d(\mu\lambda) \frac{E}{2\mu\lambda}(1-e^{-4\pi\mu}), \tag{27}$$

where E is the wave energy per unit surface area and $\frac{1}{2}E$ is the kinetic energy. $\gamma(\mu)$, which we call the energy transfer fraction, accounts for two facts. The first is that the fluid convected downward through $z = \mu\lambda$ will have less than the mean kinetic wave energy in the region above it. This occurs because the kinetic energy density is largest at the surface and diminishes with depth. Secondly, some wave energy is convected upward through $z = \mu\lambda$, although this is expected to be rather small for $\mu > 0.2$.

If there is some value of μ such that most of the wave energy is above $\mu\lambda$ and most of the wave energy loss is represented by the downward energy flux, rather than wave-to-turbulence energy transfer above $\mu\lambda$, the energy convection can be related to the wave decay rate, σ, by,

$$2\sigma E = \mathscr{Q}. \tag{28}$$

Combining (28), (27), (26) and (21), this last being reasonably valid for $\mu\lambda < 2L_1$, relates σ to the wave and turbulence parameters as

$$\sigma = \gamma(\mu)\, u' \frac{1}{11.476 L_1^{\frac{1}{3}} \mu^{\frac{2}{3}} \lambda^{\frac{2}{3}}}(1-e^{-4\pi\mu}). \tag{29}$$

Equating this expression for σ to the experimentally determined (25) leads to the following requirement on $\gamma(\mu)$:

$$\gamma(\mu) = 1.182 \frac{\mu^{\frac{2}{3}}}{1-e^{-4\pi\mu}}. \tag{30}$$

In assessing whether or not the approximation for turbulence-induced wave decay given by (25) can be explained on the basis of downward convection of energy, we inquire as to whether plausible values of γ and μ can satisfy (25). It seems that they can. For example, if $\mu \approx 0.25$ (one-quarter wavelength deep), $\gamma \approx 0.5$. Nearly all the wave energy lies above a depth of $\frac{1}{4}\lambda$. It is quite reasonable for the mean downward rate of energy convection at this depth to be half the product of the mean downward volume flux from the turbulence and the mean kinetic energy density.

7. Conclusions

The dissipation of waves of small steepness by turbulence whose horizontal component is close to homogeneous through the depth of wave energy is reasonably well approximated by equation (25) for the range of conditions of our experiments. These included waves of small steepness and wave–turbulence conditions of $4.8 < \lambda/L_1 < 7.2$ and $2.0 < f_w L_1/u' < 7.2$ except for one larger value in a case with too small a dissipation rate for its measurement to be trustworthy.

Within the range of small steepness, the damping rate is little influenced by wave steepness. Thus the wave energy loss rate is proportional to the wave energy and not to a higher power of it. When the wave steepness is large, wave–turbulence interactions may well influence micro-breaking which is a different and potentially larger dissipation mechanism.

Variations in the parameter $f_w L_1/u'$ did not influence wave dissipation in our experiments. The wave frequency range of 4 to 5.3 Hz in our experiments is about in the centre of the range of interest for Bragg scattering associated with microwave remote sensing in lakes and oceans. For the same frequencies, in natural environments differences in u' and L_1 generally result in $f_w L_1/u'$ being one or more orders of magnitude larger than in our experiments, as exemplified by the measurements of Kitaigorodskii *et al.* (1983). Similarly, natural values of λ/L_1 are much smaller than our experimental values for the same wavelength. If these parameters influence the non-dimensional dissipation rate for variations outside the range of our experiments, (25) would not be applicable to those conditions. However, if wave dissipation is governed by vertical turbulent mixing and if there is a wave/turbulence frequency ratio of importance, the important turbulence frequency would probably be w'/L_3 in the wave energy layer, where L_3 is the vertical lengthscale of the vertical turbulence velocity. In that case, the frequency ratio would be $f_w \mu^{\frac{2}{3}} \lambda^{\frac{2}{3}} L_1^{\frac{1}{3}}/u'$, where this has been obtained using the Hunt & Graham formulation for the near-surface vertical lengthscale given in the appendix of Brumley & Jirka as well as our equation (21) for w'. The wave energy layer is covered by $\mu \approx 0.25$. Many lake and ocean conditions exist for which $f_w \mu^{\frac{2}{3}} \lambda^{\frac{2}{3}} L_1^{\frac{1}{3}}/u'$ is within the range of our experiments, and we found that changing frequency ratios by a factor of three did not influence the non-dimensional decay rate. Hence, (25) may be valid for turbulence lengthscales outside the range of our experiments. Further experiments are required to determine if this is the case.

Two factors lend credence to the possibility that the dominant mechanism for the dissipation of non-breaking waves by turbulence is vertical mixing, as proposed by Boyev, and by Kitaigorodskii & Lumley. One is that the decay rate of waves of small steepness is independent of wave amplitude. If wave-to-turbulence energy transfer in the wave energy layer were the principal mechanism, we would expect the decay rate to increase with wave amplitude. The second factor is that the dissipation rates encountered have the order of magnitude expected for energy loss by vertical convection. The best way to directly assess the energy transfer by vertical mixing is to conduct experimental measurements of the correlation expressed in equation (2). Such an experiment has not, to our knowledge, been conducted.

Finally, the rough agreement between our results and those from our analysis of Skoda's data supports the findings we have made.

This work was supported, in part by the Office of Naval Research under Grant Number N00014-89-J-1185 and contract number N000144-89-J-1499. The wave tank and mechanism for oscillating the large grid were made available by the Ship Hydrodynamics Laboratory of the University of Michigan. Without these, we would have been unable to conduct the experiments.

Appendix. Analysis of the wave and turbulence data of J. D. Skoda

In this Appendix we estimate values of turbulence-induced decay rates and of turbulence mixing rate, $\mathscr{M}$, for the experiments done by Skoda (1972). His experiments were conducted in a channel 30.5 cm wide and 61 cm deep.

A.1. *Turbulence*

Turbulence was generated by two rows of transversely oscillating paddles near the bottom of the channel. Unsteady horizontal velocities were measured with a hot-film anemometer towed at 39.6 cm/s, 11.4 cm beneath the surface. Measurements were

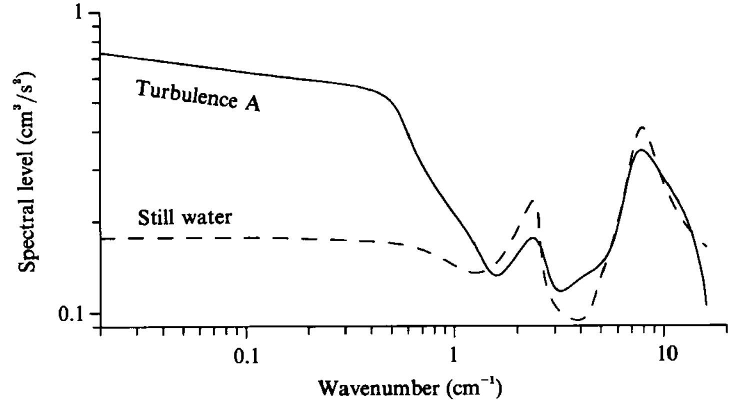

FIGURE 12. Spectral data from Skoda for still water and one turbulence condition.

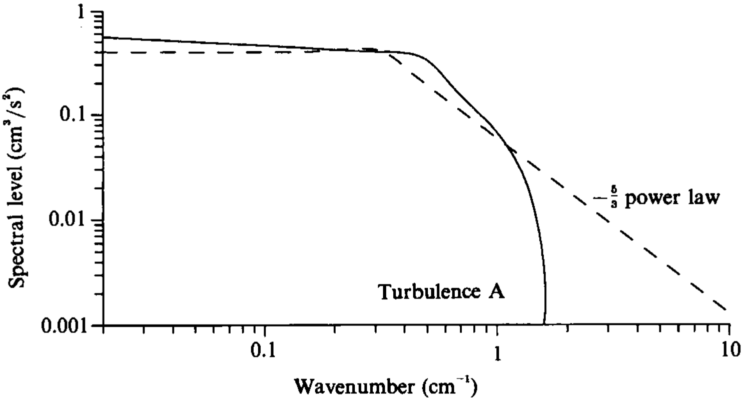

FIGURE 13. Comparison of spectra for turbulence condition A. The choices of S_0 and k_0 are somewhat arbitrary, leading to uncertainties in energy of roughly 50 % which imply uncertainties in u' of roughly 25 %. For spectra with the form of (A 1), $u' = (2.5k_0 S_0)^{\frac{1}{3}}$ and $L_1 = 0.63/k_0$. Table 3 shows the parameters for our approximations to the spectra.

taken with still water and with three turbulence conditions, labelled A, B and C. These data are presented by Skoda as graphs of their frequency spectra. We converted these to wavenumber spectra using equation (9). Figure 12 shows spectra for still water and for one turbulence condition. Three problems with these data are: the data for wavenumbers above 1 cm^{-1} (about 6 Hz) are contaminated by what is probably instrument vibration; the relatively high spectral level for the still-water condition which could be due to broadband vibration or system noise; and the slope of the spectrum for wavenumbers below the 'knee' is more than expected.

For our analysis, we estimate the actual turbulence conditions by more typical spectra, $S_a(k)$,

$$S_a(k) = \begin{cases} S_0 & (0 \leqslant k \leqslant k_0) \\ S_0(k_0/k)^{\frac{5}{3}} & (k > k_0). \end{cases} \qquad (\text{A } 1)$$

S_0 and k_0 are chosen so $S_a(k)$ resembles Skoda's turbulence spectra with the still-water spectrum subtracted from them. Figure 13 shows the comparison for turbulence condition A. The choices of S_0 and k_0 are somewhat arbitrary, leading to

Turbulence condition	k_0 ($\mathrm{cm^{-1}}$)	S_0 ($\mathrm{cm^3\,s^{-2}}$)	u' ($\mathrm{cm\,s^{-1}}$)	L_1 (cm)
A	0.32	0.40	0.56	2.0
B	0.24	2.55	1.24	2.6
C	0.24	2.79	1.29	2.6

TABLE 3. Parameters for the approximate spectra used in the analysis

uncertainties in energy of roughly 50% which imply uncertainties in u' of roughly 25%.

For spectra with the form of (A 1), $u' = (2.5k_0S_0)^{\frac{1}{2}}$ and $L_1 = 0.63/k_0$. Table 3 shows the parameters for our approximations to the spectra.

A.2. *Waves*

Skoda generated 'two-dimensional' waves with an oscillating paddle and measured their amplitudes, A_{w}, at four longitudinal locations 8, 14, 20 and 26 ft from the wavemaker. He estimated spatial decay rates by approximating the wave amplitudes at $x = 11$ and 23 ft by their surrounding values and fitting the function $A\,\mathrm{e}^{-Bx}$ to these two numbers. For our analysis of Skoda's data, we chose values for A_0 and β_{m} for each experimental run that minimized the mean-square error between the four measured values of A_{w} and the function

$$\tilde{A}_{\mathrm{w}}(x) = A_0\,\mathrm{e}^{-\beta_{\mathrm{m}}x}. \tag{A 2}$$

Measured temporal decay rates, σ_{m}, were determined from

$$\sigma_{\mathrm{m}} = \beta_{\mathrm{m}}c_{\mathrm{g}}. \tag{A 3}$$

Decay rates due to turbulence were estimated by the measured values less the rates σ_{v} and σ_{w} due to laminar dissipation within the fluid and within the sidewall boundary layers. The laminar viscous decay rate in a fluid with kinematic viscosity ν is well known as

$$\sigma_{\mathrm{v}} = 2\nu k_{\mathrm{w}}^2. \tag{A 4}$$

We calculate the decay rate of deep water waves due to laminar friction in a channel of width W as

$$\sigma_{\mathrm{w}} = \frac{(\pi\nu f_{\mathrm{w}})^{\frac{1}{2}}}{W}. \tag{A 5}$$

In the absence of surface tension, this agrees with the gravity wave result given by Ursell, Dean & Yu (1960).

The turbulence-induced decay rate is then

$$\sigma = \sigma_{\mathrm{m}} - \sigma_{\mathrm{v}} - \sigma_{\mathrm{w}}. \tag{A 6}$$

σ includes the dissipation due to turbulence in the wave layer at the surface and the turbulent augmentation to dissipation in the sidewall boundary layers. We do not know the magnitude of the latter effect in Skoda's experiments and all we can say is that, because of it, values of σ are expected to be larger than they would be without it.

Table 4 shows Skoda's values for B, in addition to β_{m}, σ_{m}, σ_{v}, σ_{w} and $u'/(L_1^{\frac{1}{3}}\lambda^{\frac{2}{3}})$.

Turb. cond.	f_w	λ	c_g	B	β_m	σ_m	σ_v	σ_w	σ	$\frac{u'}{L_1^{\frac{1}{3}}\lambda^{\frac{2}{3}}}$
A	6.70	4.08	0.584	0.128	0.128	0.0749	0.0484	0.0152	0.0113	0.175
A	5.01	6.65	0.613	0.029	0.029	0.0179	0.0182	0.0132	−0.0135	0.126
A	4.12	9.48	0.682	0.062	0.063	0.0427	0.0090	0.0119	0.0218	0.100
A	3.42	13.58	0.783	0.033	0.031	0.0246	0.0044	0.0109	0.0093	0.079
A	2.76	20.59	0.946	0.010	0.009	0.0089	0.0019	0.0098	−0.0028	0.060
A	5.17	6.26	0.606	0.160	0.161	0.0973	0.0206	0.0134	0.0634	0.132
A	3.42	13.58	0.783	0.038	0.037	0.0291	0.0044	0.0109	0.0139	0.079
A	3.56	12.60	0.760	0.040	0.050	0.0380	0.0051	0.0111	0.0218	0.083
B	6.06	4.79	0.585	0.221	0.221	0.1293	0.0352	0.0145	0.0796	0.318
B	5.00	6.65	0.614	0.294	0.294	0.1804	0.0182	0.0131	0.1490	0.255
B	4.16	9.30	0.677	0.313	0.316	0.2139	0.0093	0.0120	0.1926	0.204
B	3.42	13.58	0.783	0.052	0.047	0.0368	0.0044	0.0109	0.0216	0.158
B	2.75	20.82	0.680	—	0.027	0.0182	0.0019	0.0097	0.0066	0.119
B	6.06	4.79	0.585	0.106	0.107	0.0623	0.0352	0.0145	0.0126	0.318
B	6.70	4.09	0.584	0.148	0.148	0.0866	0.0482	0.0152	0.0232	0.353
B	4.02	9.92	0.693	0.063	0.061	0.0421	0.0082	0.0118	0.0222	0.195
B	3.42	13.58	0.783	0.051	0.050	0.0390	0.0044	0.0109	0.0237	0.158
B	2.75	20.82	0.680	0.029	0.028	0.0193	0.0019	0.0097	0.0077	0.119
B	4.24	8.99	0.669	0.048	0.030	0.0203	0.0100	0.0121	−0.0017	0.209
B	3.43	13.49	0.783	0.081	0.082	0.0642	0.0044	0.0109	0.0489	0.159
B	3.44	13.39	0.783	0.069	0.098	0.0770	0.0045	0.0109	0.0616	0.160
C	4.06	9.77	0.689	—	0.000	0.0000	0.0085	0.0118	−0.0203	0.205
C	5.02	6.60	0.613	—	0.037	0.0224	0.0185	0.0132	−0.0092	0.267
C	4.21	9.08	0.673	0.104	0.105	0.0704	0.0098	0.0121	0.0485	0.216
C	3.42	13.58	0.783	0.008	0.104	0.0814	0.0044	0.0109	0.0662	0.165
C	3.80	11.07	0.720	0.049	0.049	0.0354	0.0066	0.0115	0.0174	0.189
C	6.15	4.67	0.584	0.110	0.135	0.0787	0.0370	0.0146	0.0272	0.336
C	3.44	13.58	0.783	0.066	0.095	0.0747	0.0044	0.0109	0.0594	0.165
C	3.47	13.12	0.776	0.066	0.066	0.0509	0.0047	0.0110	0.0353	0.169

TABLE 4. Results of analysis of the data of Skoda (1972). The printing for the values of B in Skoda's thesis are difficult to read: those that could not be discerned are left blank and others may be in error.

The ordering of rows of results in table 4 is the same as Skoda's Appendix C. These results, in the form of σ *vs.* $\mathscr{M}$, are shown in figure 11.

REFERENCES

BOYEV, A. G. 1971 The damping of surface waves by intense turbulence. *Izv. Atmos. Ocean Phys.* **7**, 31–36.

BRUMLEY, B. H. & JIRKA, G. H. 1987 Near surface turbulence in a grid-stirred tank. *J. Fluid Mech.* **183**, 235–263.

GREEN, T., MEDWIN, H. & PAQUIN, J. E. 1972 Measurements of surface wave decay due to underwater turbulence. *Nature, Phys. Sci.* **237**, 115–117.

HUNT, J. C. R. & GRAHAM, J. M. R. 1978 Free stream turbulence near plane boundaries. *J. Fluid Mech.* **84**, 209–235.

JENKINS, G. M. & WATTS, D. G. 1968 *Spectral Analysis and its Applications.* Holden-Day.

KITAIGORODSKII, S. A., DONELAN, M. A., LUMLEY, J. L. & TERRAY, E. A. 1983 Wave–turbulence interactions in the upper ocean. Part II. Statistical characteristics of wave and turbulent components of the random velocity field in the marine surface layer. *J. Phys. Oceanogr.* **13**, 1988–1998.

KITAIGORODSKII, S. A. & LUMLEY, J. L. 1983 Wave–turbulence interactions in the upper ocean. Part I. The energy balance of interacting fields of surface wind waves and wind-induced three-dimensional turbulence. *J. Phys. Oceanogr.* **13**, 1977–1987.

MCDOUGALL, T. J. 1979 Measurements of turbulence in a zero-mean-shear mixed layer. *J. Fluid Mech.* **94**, 409–431.

PHILLIPS, O. M. 1958 The scattering of gravity waves by turbulence. *J. Fluid Mech.* **5**, 177–192.

SAVITSKY, D. 1970 Interaction between gravity waves and finite turbulent flow fields. In *Proc. 8th Symp. on Naval Hydrodynamics*. Office of Naval Research, *California Institute of Technology*.

SKODA, J. D. 1972 The interaction of waves and turbulence in water. Ph.D. thesis, University of California, Berkeley.

URSELL, F., DEAN, R. G. & YU, U. S. 1960 Forced small-amplitude water waves: a comparison of theory and experiment. *J. Fluid Mech.* **7**, 33–52.